Q. J. R. Meteorol. Soc. (2000), **126**, pp. 1301–1320

Density currents in two-layer shear flows

By MING XUE*
University of Oklahoma, USA

(Received 23 April 1999; revised 22 September 1999)

SUMMARY

An earlier two-fluid model of an idealized density-current in low-level shear is extended to include variable upper-level shear. Far-field solutions are determined, based on the conservation of mass, momentum and vorticity, and the conservation of Bernoulli function (energy) along streamlines for inviscid flows. It is found that the upper-level and low-level shears play similar roles in controlling the depth of steady-state density-currents. In most cases, large positive upper-level shear supports a deeper density-current and steeper front, and therefore a stronger updraught. It is also found that when the low-level shear is weak and upper-level shear occupies about half the domain depth, larger positive shear can result in a shallower rather than a deeper density-current. This behaviour was not found for either constant shear flow or flows with only low-level shear. The behaviour is understood by examining the flow structure and flow-force components as a function of the upper-level shear. Furthermore, by allowing the upper-level shear to vary, an overturning flow is permitted ahead of the density current. This was not possible in the earlier model in which the upper-level flow was assumed to be constant. The present extension allows us to draw closer analogues between the model solutions and the circulation patterns found in typical squall-lines in sheared enviromnents.

Time-dependent numerical experiments are conducted for a range of upper- and low-level shears. The depth and the propagation speed of simulated density-currents are found to agree very well with predictions by the idealized theoretical model. This verifies the validity of the theoretical model. In addition, numerical experiments with identically zero low-level shear but differing upper-level shears suggest that the deeper shear is as important as the low-level shear in determining the uprightness of the upward branch of inflow. In fact, the presence of positive low-level inflow shear may not be essential. Such results are also supported by the theoretical model, and may have important implications for our understanding of squall-line dynamics.

KEYWORDS: Density current Squall-line dynamics

1. INTRODUCTION

It is commonly accepted that the interaction between environmental shear and the cold pool of a thunderstorm outflow (density current) may play an important role in producing long-lived squall-lines (Moncrieff 1978, 1992; Thorpe *et al.* 1982 [called from here on TMM82]; Xu and Chang 1987; Rotunno *et al.* 1988 [RKW88]; Fovell and Ogura 1988; Xue 1990). Density currents also occur in the atmosphere in other forms, such as sea-breeze fronts (e.g. Simpson *et al.* 1977) and those associated with cold frontal rain-bands (e.g. Carbone 1982). Detailed observational studies have also revealed the importance of density-current-type sea-breeze and cold-outflow fronts in the initiation and organization of convection (e.g. Weckworth and Wakimoto 1992; Atkins *et al.* 1995).

To improve our understanding of the interaction between density currents and their environment, simple nonlinear, two-fluid steady-state models were developed by Xu (1992) [X92], Xu and Moncrieff (1994) [XM94], and Liu and Moncrieff (1996a). These models include four more elements than the classic inviscid density-current theory of Benjamin (1968), namely constant environmental shear, internal cold-pool circulation, negative-vorticity generation associated with energy loss along the interfacial layer between the density current and its environment, and density stratification and latent heating. These idealized models show, through mathematical analyses, how the depth, propagation speed and shape of the density current are controlled or influenced by the environmental shear and cold-pool strength.

* Corresponding address: School of Meteorology, University of Oklahoma, Sarkeys Energy Center, 100 East Boyd, Norman, Oklahoma 73019, USA.

Laboratory experiments (e.g. Simpson 1969), observations (e.g. Wakimoto, 1982; Mueller and Carbone 1987) and numerical simulations (e.g. Droegemeier and Wilhelmson 1987) all indicate that Kelvin–Helmholtz (KH) waves and turbulent mixing often develop along the density-current interface. Therefore, one may question to what extent the idealized models of inviscid flows are valid for more realistic situations, where transient turbulent eddies are allowed to develop. Xu *et al.* (1996) [XXD96] answered this question, at least partially, using carefully designed numerical experiments. The head-depth and propagation speed of the simulated density-currents in constant shear flows were found to agree very well with theoretical predictions, and a reduced current-depth was found to the rear of the current head where active turbulence existed. The dependence of the density-current depth on the environmental shear was also examined numerically by Chen (1995) and Liu and Moncrieff (1996b). Their results support the theoretical results of X92, XM94 and Liu and Moncrieff (1996a) in general.

Xue *et al.* (1997) [XXD97] extended X92's theoretical density-current model for a constant shear flow to one in which the inflow shear is confined to the lower levels (see their Fig. 1) while the inflow above is uniform. Such a configuration possesses greater relevance to squall-line models in which strong environmental shear is often confined to the lowest few kilometres of the troposphere (TMM82; RKW88).

XXD97 found that a low-level shear controls the depth of a steady-state density-current in much the same way as a uniform vertical shear. When the shear enhances the low-level flow against the density-current propagation (shear vector pointing in the direction of propagation), the current is deeper than half of the domain depth. They conducted time-dependent numerical experiments or a variety of parameter settings, including various depths and strengths of the shear layer; the results confirm the theoretical analyses.

There are, however, a few important limitations in XXD97's model for low-level constant shears. As discussed in subsection 2(b) of their paper, for large positive (assuming the current propagates in the positive x direction) values of low-level inflow shear, solution ceases to exist as the shear depth approaches the domain depth, so that the limiting solution for a uniform shear in the entire depth can not be reached. In fact, some solution curves terminate in the middle of the figure for large positive and deep low-level shear. This behaviour stems from the upper-level flow having zero shear. To ensure the velocity continuity across the interface between the lower and upper layers, the upper-level flow has to have the same sign as the low-level flow, i.e. no flow reversal is allowed at the upstream boundary. This is not true, however, for the model of uniform shear, where flow reversal is permitted.

XXD97 hypothesized that upper-level flow reversal at the upstream boundary was possible only when the upper-level flow had non-zero shear. It should be possible to obtain steady-state far-field solution for a flow containing two shear-layers, and the solution should lie between the solutions from the constant shear and the low-level shear case. It is the purpose of the present paper to show that this hypothesis is indeed true.

In the following, we shall first develop a theoretical model of density currents in a two-layer shear flow. The far-field solutions away from the density-current head are obtained by applying the conservation laws of mass, momentum and vorticity and the conservation of Bernoulli function (energy) along streamlines, just as X92 and XXD97 did for constant and low-level shear. The theoretical results are supported by numerical experiments in sections 3 and 4. Discussions and conclusions are given in section 5.

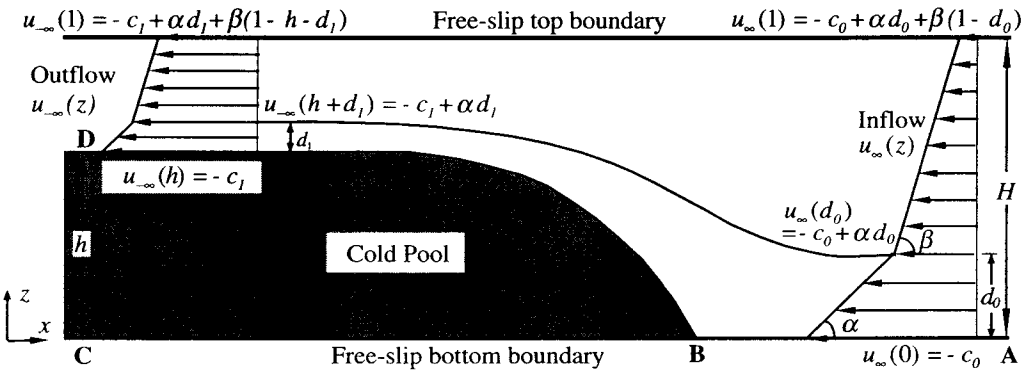

Figure 1. Schematic of the steady-state model of a density-current circulation in an environmental flow with two layers of constant shear. The remote system-relative inflow and outflow are indicated by $u_{\infty}(z)$ and $u_{-\infty}(z)$ respectively, and h is the depth of the density current. Other variables are defined in the text.

2. Density current in a two-layer shear-flow

(a) *Flow configuration and scaling*

Consider an idealized steady-state density-current propagating in an environmental flow with two constant-shear layers. The model is illustrated in Fig. 1. It has one more control parameter than the constant low-level-shear model of XXD97: the magnitude of the upper-level shear, β.

The independent and dependent variables in this model are nondimensionalized using the scaling

$$(x, z) \leftarrow (x, z)/H, \quad (u, w) \leftarrow (u, w)/U, \quad p' \leftarrow p'/(\rho_0 U^2), \tag{1}$$

where the variables on the left-hand side of the arrows are nondimensional.

In (1), x and z are the horizontal and vertical co-ordinates, u and w are the horizontal and vertical velocities, respectively, H is the depth of the domain bounded by two rigid boundaries, $U \equiv (gH\Delta\rho/\rho_0)^{1/2}$ is the velocity scale, g is the acceleration under gravity; $\Delta\rho = \rho_1 - \rho_0$ is the density difference between the denser fluid inside the cold pool ρ_1 and the lighter fluid outside ρ_0, and $p' \equiv P - P_0$ is the perturbation pressure, which is the difference between total pressure P and reference pressure P_0. The reference pressure P_0 is the unperturbed pressure in the upstream inflow associated with constant density ρ_0, where ρ_0 satisfies the hydrostatic relation $P_0 = g\rho_0(H - z)$.

In the following subsections, steady-state far-field solutions are sought for this flow configuration. The results will show how the propagation speed and cold-pool depth depend on the inflow shear. The local structure of the front will also be briefly discussed.

(b) *Model for far-field solutions*

In Fig. 1, the shaded area indicates the cold pool of an idealized density-current. Viewed in a framework moving with the density-current front, the low-level environmental flow moves towards the head from the right (upstream). The shaded area represents a semi-infinitely long cold-pool with zero internal circulation. The flow outside the cold pool is separated into two layers, each with a constant vorticity. This constant vorticity dictates that the horizontal flow far down stream has the same shear as that far upstream in both the upper and lower layer.

According to Fig. 1, the inflow profile (horizontal wind speed) is

$$u_{\infty}(z) = \begin{cases} -c_0 + \alpha d_0 + \beta(z - d_0) & \text{for } d_0 < z \leqslant 1 \\ -c_0 + \alpha d_0 + \alpha(z - d_0) & \text{for } 0 \leqslant z \leqslant d_0. \end{cases} \tag{2}$$

The outflow profile is given by

$$u_{-\infty}(z) = \begin{cases} -c_1 + \alpha d_1 + \beta(z - h - d_1) & \text{for } h + d_1 < z \leqslant 1 \\ -c_1 + \alpha d_1 + \alpha(z - h - d_1) & \text{for } h \leqslant z \leqslant h + d_1. \end{cases} \tag{3}$$

Here, α and β are, respectively, the constant lower- and upper-level shears of the environmental inflow. The quantity d_0 ($0 \leqslant d_0 \leqslant 1$) is the depth of the lower layer far upstream and c_0 (>0) the constant inflow speed (absolute value) at the lower boundary. The depth d_1 is that of the lower shear-layer above the cold pool far downstream, and c_1 (>0) is the speed of outflow atop the cold pool. Finally, h ($0 < h < 1$) is the depth of the density-current head.

It can be seen from (2) and (3) that the flow is fully described by a set of seven nondimensional control parameters

$$\{\alpha, \beta, d_0, c_0, d_1, c_1, h\} \tag{4}$$

whose definitions are given above.

Following the discussion by Benjamin (1968), the remote system-relative environmental inflow and outflow are constrained by mass continuity, vorticity conservation, and flow-force balance and the conservation of Bernoulli energy along streamlines. It can be shown that only three of the seven parameters in (4) are independent, and physical solutions can be found given any three of them. In the present paper, we shall discuss only the cases where the shears of inflow (α and β) and the height of the inflow-layer interface (d_0) are prescribed. The ground-level inflow speed (c_0), the depth of density current (h), and the outflow speed (c_1) and layer depth (d_1) will be determined by the theoretical model.

Mass continuity requires that the inflow mass flux equal the outflow mass flux, for each of the two shear layers. Using the u profiles in (2) and (3), we can obtain the following two mass-continuity constraints for the lower and upper layers, respectively:

$$d_0(c_0 - \alpha d_0/2) = d_1(c_1 - \alpha d_1/2), \tag{5}$$

and

$$(1 - d_0)\{c_0 - \alpha d_0 - (1 - d_0)\beta/2\} = (1 - d_1 - h)\{c_1 - \alpha d_1 - (1 - d_1 - h)\beta/2\}. \tag{6}$$

Furthermore, for a steady-state flow, the Bernoulli energy ($p' + v^2/2$) is constant along a streamline. Applying this theorem along the interfacial streamline from the frontal nose B to the downstream point D, and along the lower boundary from B to C, noting that the flow speed is zero at B (stagnation point) and C (no flow inside the cold pool), and making use of the hydrostatic equation between D and C (see XXD97 for more details), we obtain another constraint among the control parameters

$$c_1 = \sqrt{2h}. \tag{7}$$

Integrating the steady-state horizontal-momentum equation over the entire domain and making use of mass continuity, as did XXD97, we obtain the flow-force (pressure–momentum force integral, see Benjamin 1968) balance

$$\int_0^1 (p'_{\infty} + u^2_{\infty})\,\mathrm{d}z = \int_0^1 (p'_{-\infty} + u^2_{-\infty})\,\mathrm{d}z. \tag{8}$$

By applying the Bernoulli theorem again along the lower boundary streamline through point A and point B, one can obtain

$$p'_{\mathrm{B}} = p'_{\mathrm{A}} + c_0^2/2 = c_0^2/2 \tag{9}$$

where we have assumed $p'_{\mathrm{A}} = 0$. Given that $\Delta\rho_{\infty} = 0$, we have, according to the hydrostatic relation $\partial p'/\partial z = 0$:

$$p'_{\infty}(z) = p'_{\mathrm{A}} = 0. \tag{10}$$

On the outflow boundary, p' is again obtained by integrating the hydrostatic relation vertically, making use of (9)

$$p'_{-\infty}(z) = \begin{cases} c_0^2/2 - z & \text{for } 0 \leqslant z \leqslant h \\ c_0^2/2 - h & \text{for } h \leqslant z \leqslant 1. \end{cases} \tag{11}$$

Substituting velocity profiles in (2) and (3) and pressure profiles in (10) and (11) into (8), we obtain the flow-force balance constraint

$$\begin{aligned} &-(c_0 - \alpha d_0)^2 + 2(c_1 - \alpha d_1)^2(1-h) \\ &\quad - (2-h)h + 2(c_1 - \alpha d_1)d_1^2\alpha - \{d_0^2(2d_0 - 3) - 2d_1^3\}\alpha^2/3 \\ &\quad - 2(c_1 - \alpha d_1)(1 - d_1 - h)^2\beta + 2(c_0 - \alpha d_0)(1 - d_0)(d_0\alpha + \beta - d_0\beta) \\ &\quad + 2(d_0 - d_1 - h)\{d_0^2 - 2d_0 + (3 - d_0)(1 - d_1 - h) + (d_1 + h)^2\}\beta^2/3 = 0. \end{aligned} \tag{12}$$

Now we have four constraints, given in (5), (6), (7) and (12), for seven control parameters, only three of which are free. We now eliminate c_0 among (5) and (6) and obtain

$$\begin{aligned} 2c_1\{d_1 - d_0(1-h)\} = &\{d_0^2 - d_0^3 + d_1^2 - d_0d_1(2 - d_1 - 2h)\}\alpha \\ &-d_0(d_0 - d_1 - h)(2 - d_0 - d_1 - h)\beta, \end{aligned}$$

which can be re-written as a quadratic equation in d_1

$$A_2 d_1^2 + A_1 d_1 + A_0 = 0 \tag{13a}$$

where

$$A_2 \equiv \{\alpha + d_0(\alpha - \beta)\}/2, \tag{13b}$$

$$A_1 \equiv -c_1 - \alpha d_0(1-h) + \beta d_0(1-h), \tag{13c}$$

$$A_0 \equiv d_0\{2c_1(1-h) + d_0(\alpha - \beta)(1 - d_0) - \beta(d_0 - 2h + h^2)\}/2. \tag{13d}$$

It can be verified that when $\beta = 0$, the above equation reduces to that for the low-level shear case discussed by XXD97.

We seek to find sets of the seven parameters that satisfy all four constraints. Since we are most interested in how the environmental flow profile affects the density current, including its depth and propagation speed, we choose to specify the three parameters α, β and d_0, that define the upstream flow profile. Note that these three parameters define only the shape of the profile. The speed, represented by c_0, remains to be determined. We seek the solutions of the other four parameters numerically. The procedure is as follows. For given values of α, β and d_0, $(1 > d_0 > 0)$, we solve for (c_0, c_1, h, d_1):

1. loop over all physical values of h ($1 > h > 0$);
2. compute c_1 from (7);
3. solve for d_1 from (13a–d):

$$d_{1\pm} = -0.5A_1/A_2 \pm 0.5(A_1^2 - 4A_2A_0)^{1/2}/A_2 \tag{14}$$

and keep only root(s) in the range $1 - h \geqslant d_1 \geqslant 0$;
4. check to see if (2) is satisfied;
5. finally obtain c_0 from either (5) or (6).

(c) *Far-field solutions*

This procedure gives only one set of physical solutions that satisfies the four constraints. It corresponds to the second root of d_1 (d_{1-}) in (14) and reduces, in the limit of constant inflow ($\alpha = \beta = 0$), to the energy-conserving solution of Benjamin (1968), to that of X92 in the limit of constant inflow shear ($\alpha = \beta \neq 0$), and to the solution of XXD97 when only the low-level shear is non-zero ($\alpha \neq 0$, $\beta = 0$). Selected solutions are plotted in Figs. 2, 3 and 4.

In Fig. 2, the cold-pool depth h and the ground-level (density-current) front-relative inflow speed c_0 are plotted against the low-level inflow shear α for the values of depth d_0 ranging between 0.1 and 0.9 and for a fixed value of $\beta = -0.5$. Figure 3 shows the same parameters, except that $\beta = +0.5$, and Fig. 4 shows how the density-current depth h varies with β for the various values of d_0 and two different values of α.

Figures 2(a) and 3(a) correspond to Fig. 2 of XXD97 and Figs. 2(b) and 3(b) correspond to Fig. 3 of that paper where $\beta = 0$. (Note that c_0 there is defined as the upper-level rather than the surface flow speed.) The dependency of the density-current depth and propagation speed on the low-level shear is in general agreement with both the uniform shear and the low-level shear cases discussed in X92 and XXD97. The density current becomes deeper and propagates faster relative to the surface environmental flow as the low-level inflow shear increases from negative to positive values.

Combination of the present results with those of XXD97 shows that negative upper-level shear (β) gives a shallower current (Fig. 2 of the present paper) than low-level shear alone ($\beta = 0$, Figs. 2 and 3 of XXD97), and that relatively small positive upper-level shears have the opposite effect (Fig. 3 of the present paper). For $\alpha = 0$ and $d_0 = 0.2$, for example, the value of h increases from +0.42 when $\beta = -0.5$ (Fig. 2 of the present paper), to +0.5 when $\beta = 0$ (Fig. 2 of XXD97) and to +0.58 when $\beta = +0.5$ (Fig. 3 of the present paper). For the second case ($\alpha = \beta = 0$) the inflow is constant, and the solution degenerates to the classic inviscid density-current solution ($h = 0.5$, $c_0 = 0.5$) of Benjamin (1968).

Now consider Fig. 4, where h is plotted against β for various values of the upper-level shear ($1 - d_0$) and for $\alpha = 1$ and $\alpha = 0$. When $\alpha = 1$ (Fig. 4(a)), and β is in the range where valid solutions may be found, h increases monotonically with β for all depths of the upper-level shear, and the effect of shear is enhanced for successively deeper depth. When $\alpha = 0$ (Fig. 4(b)), the relationship becomes less simple. For intermediate values of shear depth, h begins to decrease with increasing positive shear and a peak value of h occurs around $\beta = 2$. This behaviour is most pronounced for intermediate values of shear depth. The non-monotonic relationship between h and β also occurs for negative values of α (not shown), and the general behaviour is similar to the previous example. The ground-level inflow speed c_0 (not shown), however, increases with increased upper-level shear in all cases.

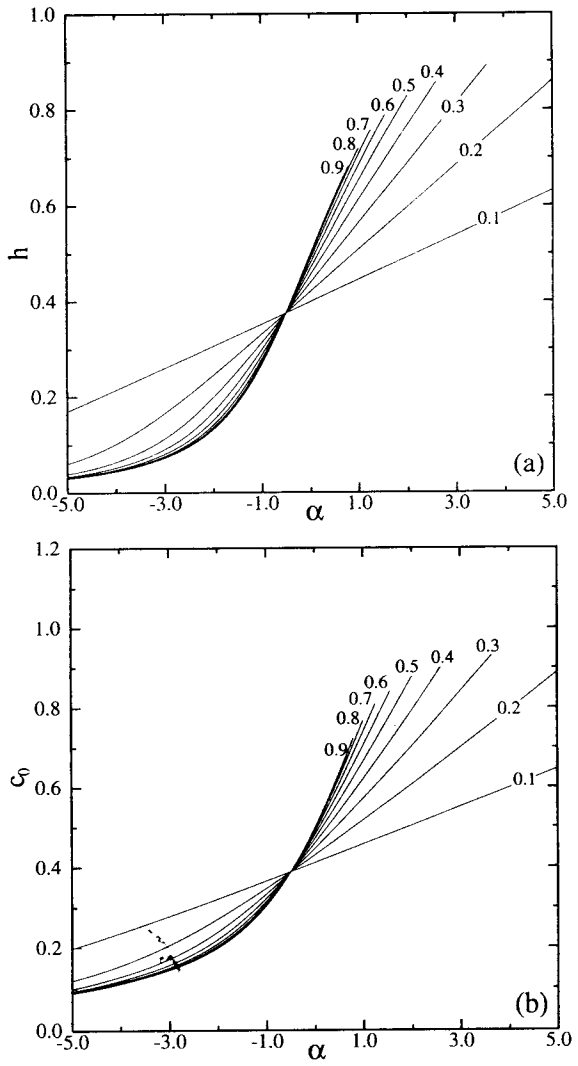

Figure 2. Variation with inflow shear α for values of lower-layer-shear depth d_0 in the range 0.1 to 0.9 according to the steady-state theoretical model: (a) cold-pool depth h; (b) front-relative ground-level inflow speed c_0 (i.e., the current-propagation speed). The upper-layer shear β is negative and equal to -0.5.

The non-monotonic relationship between h and β for intermediate values of d_0 and small or negative values of α may be understood by examining the flow structures for different values of β. When β is positive and large, strong overturning flow develops upstream so that a significant portion of the inflow in the lower part of the upper shear layer leaves via the upper-level upstream boundary. The low-level weakly-sheared flow decelerates as it passes over the cold pool, resulting in positive pressure-anomalies (as a result of the Bernoulli effect). The positive pressure-anomalies push down the cold pool, resulting in shallower density-currents. A set of numerical experiments has been conducted that confirms this behaviour.

To see when overturning occurs, consider Fig. 5 which shows the flow speed at the upstream top boundary $\{-u_\infty(z = 1)\}$ as a function of upper-level shear β and its

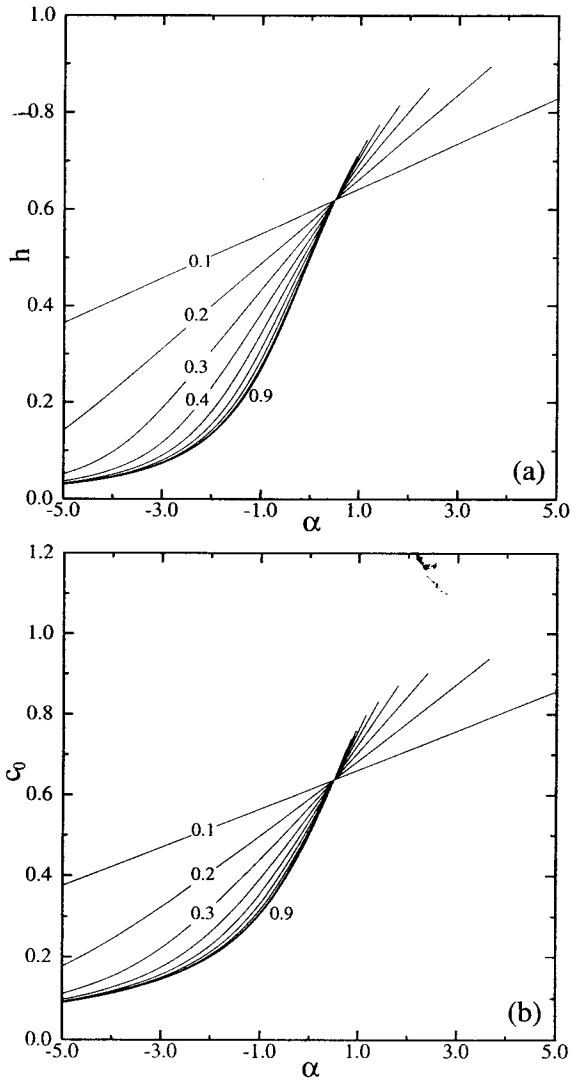

Figure 3. As Fig. 2, but with upper-level shear β equal to +0.5.

depth $(1 - d_0)$ for a fixed positive value of low-level shear ($\alpha = 1$). For a typical value of $(1 - d_0)$, 0.9 say, upper-level overturning flow ($-u_\infty < 0$) starts to appear in the upstream inflow when β exceeds about 0.8 and the overturning is stronger for larger β. We shall see later that this agrees with the numerical results (see section 4).

So, moderately strong upper-level shear plays a role similar to that of the low-level shear in raising the density-current head whereas negative upper-level shear reduces it. Moreover, when the assumption of constant upper-level flow is removed, the flow at both the top and the bottom of the upper-layer can be directed inward as well as outward at the right boundary for certain values of α and β, so removing a limitation of the low-level shear model of XXD97.

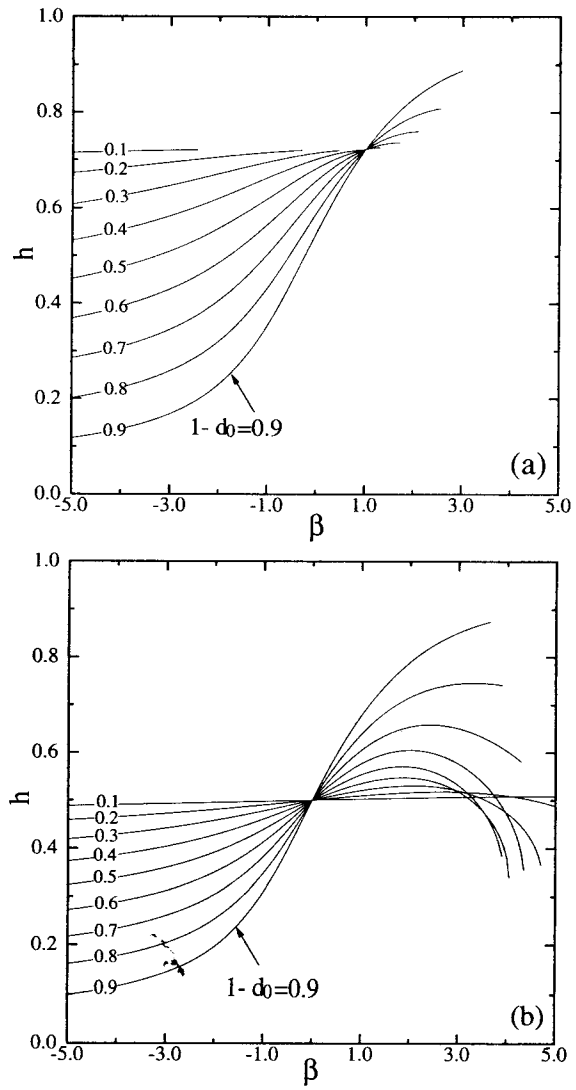

Figure 4. The density-current depth h from the theoretical model for different depths of the upper shear layer plotted against the upper-level shear β: (a) for low-level shear $\alpha = 1$; (b) for low-level shear $\alpha = 0$. The depth of the upper layer $(1 - d_0)$ is labelled on the corresponding curves.

Further physical understanding of these solutions may be gained by analysing the behaviour of flow-force balance under the conditions of mass, vorticity and Bernoulli energy conservation, as was done by X92.

(*d*) *Local and global structures of the front*

The flow structure near the front is as important as the far-field solutions discussed earlier. The shape of the front of a thunderstorm outflow, for instance, has a direct influence on the vertical orientation of the low-level updraught. An upshear-tilted updraught allows condensed water to be downloaded underneath the updraught without

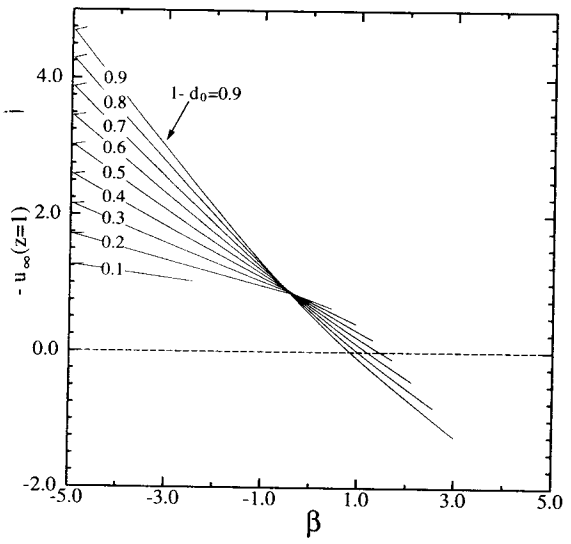

Figure 5. The flow speed $-u_\infty$ at the upstream top boundary ($z = 1$) as a function of the shear β and depth $(1 - d_0)$ of the upper-level flow. Negative values of $-u_\infty$, below the pecked line, indicate outflow.

interrupting the low-level inflow, allowing long-lived squall-line-type convection to be maintained (e.g. TMM82; RKW88).

Von Kármán (1940) and Benjamin (1968) showed analytically that the angle at the stagnation point between the density front and the horizontal is 60° for an idealized inviscid density-current in a uniform (non-sheared) environmental flow with a free-slip lower boundary condition. X92 and XM94 showed, further, that this 60° angle is independent of the inflow shear and cold-pool circulation.

The shape of the frontal interface is determined by the continuity condition of pressure across the interface and the solution can be obtained numerically. According to X92 and XM94, when the positive inflow shear is very strong, the frontal interface slope can become steeper than 60° at the mid-depth ($z = h/2$) location. We may expect that these findings can be extended to the two-layer shear-flow model discussed in the present paper.

The next section presents the results from the numerical experiments and discusses them.

3. THE NUMERICAL MODEL AND EXPERIMENT DESIGN

(*a*) *The numerical model*

A modified version of the Advanced Regional Prediction System (ARPS) (Xue *et al.* 1995) is used for our numerical experiments, as it was by XXD97. It is used in its simplest dry two-dimensional mode, with no 'physics'. To facilitate direct comparison of numerical results with the theoretical solutions, the Boussinesq approximation is assumed. The base-state density ρ_0 and potential temperature θ_0, are set to constant values. At the top and bottom boundaries, rigid free-slip conditions are applied. Wave-radiation conditions are used at the lateral boundaries. Further details were given by XXD97.

Following XXD97, sub-grid scale turbulence parametrization is not included. Instead, high spatial resolution is relied upon to resolve the turbulent eddies often found

to the rear of the current head. Only a small amount of horizontal computational mixing/diffusion is applied, and on the velocity fields only. Vertical mixing is not used for fear of affecting the vertical wind profile.

To improve the accuracy of numerical solution further, in the present paper the monotonic flux-corrected transport (FCT) scheme of Zalesak (1979) is applied to the advection of potential temperature field. This scheme prevents spurious extrema from developing near sharp gradient (across the cold-pool interface) and therefore removes the need for explicit numerical diffusion of potential temperature.

(*b*) *Model scaling and initial conditions*

The equations solved by the model are those for horizontal velocity u, vertical velocity w, perturbation pressure p' and perturbation buoyancy b in nondimensional form, as given by XXD97 in their Eq. (3.1). The scaling parameters used by XXD97 are also used here in nondimensionalizing the model equations, viz., length scale H (the domain depth), velocity scale $U \equiv (gH\Delta\rho/\rho_0)^{1/2}$, pressure scale $P \equiv \rho_0 U^2 = gH\Delta\rho$, time scale $T \equiv H/U$ and buoyancy scale $B \equiv g\Delta\rho/\rho_0 = g\Delta\theta/\theta_0$. In the dimensional ARPS model, we choose for convenience $H = 1$ km, $\Delta\theta = 3$ K, $\theta_0 = 300$ K, $g = 10$ m s^{-2}. The other derived scaling parameters are $U = 10$ m s^{-1}, $P = 120$ Pa and $T = 100$ s. Since our results will be presented and discussed in nondimensional space, the results are not limited to the applications of shallow domain.

The density current in the numerical model is generated by placing an initially static block of cold air ($b = -1$) in the middle portion of an elongated computational domain of size 40×1 nondimensional units consisting of 767×81 grid points. Therefore, the grid spacings are $\Delta x = 0.05$ and $\Delta z = 0.0125$ in the horizontal and vertical directions respectively. This domain is long enough for the upstream boundary flow to remain undisturbed throughout the integration period, while disturbances that reach the downstream boundary can propagate freely out of the domain. The cold pool thus specified is, in most cases, able to supply sufficient cold air for achieving and maintaining a quasi-steady density-current. The initial shape of the cold pool is that specified by XXD97 (cf. their Eq. (3.3)). The interface has a slope of 60° at the frontal nose.

The initial flow at the far upstream and downstream boundaries is specified according to (2) and (3). This automatically ensures the flow-force balance between the two boundaries at the initial time. The upstream shears α and β and the lower-layer depth d_0 are specified as the control parameters. The corresponding density-current depth h and the ground-level inflow speed c_0 for a steady-state current can be found from Figs. 2, 3 and 4.

The initial flow in the interior is obtained by solving a vorticity equation numerically. Because the vorticity distribution depends on the solution of the stream function, the right-hand side of the equation is adjusted in an iterative procedure. More details of the solution procedure were given by XXD97 and an example of the initial flow for positive low-level and negative upper-level shear is given in Fig. 6 of the present paper, corresponding to one of the experiments presented later.

Finally, let us specify the initial cold block to be wider than 8 nondimensional units, so that the cold-air supply may be sufficient for a steady-state solution to evolve and be maintained. This was discussed further by XXD97.

(*c*) *Experimental design*

The main purpose of the present numerical experiments is to examine the validity of the theoretical results obtained in the previous section; in particular, to see if a

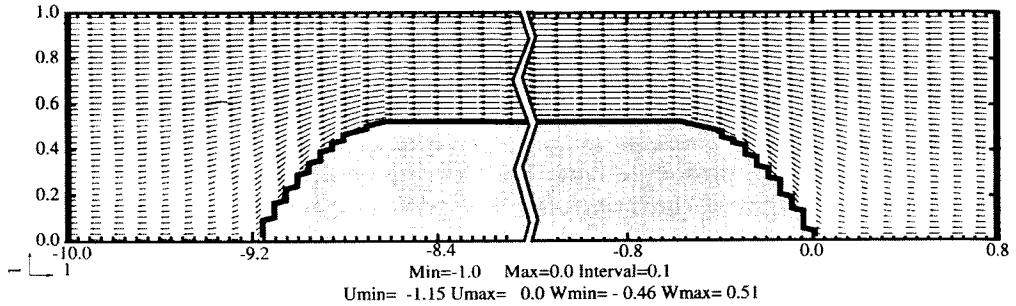

Figure 6. Initial configuration of cold pool and outside flow for $\alpha = 1$, $\beta = -0.5$, $d_0 = 0.2$ and $h = 0.51$. The far-field flow satisfies the theoretical steady-state solution for the given set of parameters. The right and left portions of the initial cold-pool have horizontal and vertical scales chosen to present a physically correct shape. The mid-portion of the cold pool is omitted. Note that the domain is nondimensional. The x-axis origin is located at the right frontal nose at the initial time. The horizontal- and vertical-velocity scales ($w = u = 1$) are shown by the arrow at the lower left-hand corner.

quasi-steady-state density-current circulation can be established in a time-dependent numerical model, and if so, how well the numerical result agrees with the theoretical solution. In addition, the numerical model provides a solution in the current-head region. For these purposes, the seven experiments listed in Table 1 were carried out.

The experiments are named according to the lower and upper-level shear in the environmental inflow. For example, experiment L1UM2 has a low-level shear $\alpha = 1$ and an upper-level shear $\beta = -2$. Here character M denotes the minus sign. As discussed earlier, the interaction between density current/cold outflow and low-level shear is an important issue for storm initiation and evolution. Consequently, all experiments assume an inflow-layer interface that is at 0.2 of the domain depth, i.e. $d_0 = 0.2$. If the top boundary is at the tropopause, the interface is at about 2 km. If the rigid top represents an inversion cap of a planetary boundary-layer of 2 km deep, 0.2 represents a 400 m low-level shear-layer, which is often present as a result of surface friction. The $d_0 = 0.2$ setting is also used in most of the experiments reported by XDD97.

In the first set of (five) experiments, the low-level shear α is $+1$, while the upper-level shear β varies from $+2$ to -2 by increments of one. In another word, the shear changes from being moderately strong positive to moderately strong negative. For L1U1, the inflow has a uniform shear of one, corresponding to the situations examined by XXD96. In L1U0, the inflow has a low-level shear only, corresponding to one of the low-level shear cases examined by XXD97 (their experiment LS 1).

In the second set of (two) experiments, the low-level shear is set at zero while the upper-level shear is 2 and -2, corresponding to the moderately strong positive and negative upper-level shears in the first set. This second set allows examination of the relative role of low-level shear in determining the head depth and the slope of the frontal zone, and hence the orientation of the updraught at the front.

In all cases, the initial inflow profiles are set according the theoretical steady-state model, as are the initial cold-pool depths. XXD96 and XXD97 showed that the final quasi-steady state of the numerical solutions is independent of the initial depth of the cold pool, as long as sufficient cold air mass is available.

The initial flow is set up using the procedure discussed earlier so that it matches the theoretical model solution closely. The initial flow adjustment is therefore minimized and we may expect the upstream front to remain quasi-stationary and the cold-pool

TABLE 1. INITIAL SETTINGS AND SIMULATED PARAMETER VALUES FOR THE NUMERICAL EXPERIMENTS

Experiment	Model specified settings			Theoretical values		Model simulated values	
	α	β	d_0	h	c_0	h	c_0
1. L1U2	1	2	0.2	0.79	1.06	0.76	1.04
2. L1U1	1	1	0.2	0.72	0.80	0.68	0.79
3. L1U0	1	0	0.2	0.59	0.59	0.53	0.58
4. L1UM1	1	−1	0.2	0.43	0.46	0.39	0.45
5. L1UM2	1	−2	0.2	0.32	0.40	0.29	0.38
6. L0U2	0	2	0.2	0.72	0.97	0.68	0.95
7. L0UM2	0	−2	0.2	0.25	0.32	0.20	0.30

depth to maintain its initial height throughout the simulation. Transient activities may be expected behind the current head because of KH instability.

To compare the simulated density-currents with the idealized model, choose the left boundary of the control volume at a location where the flow interface becomes more or less horizontal and KH eddies are insignificant. This choice is dictated mainly by the constraint of the conservation of Bernoulli function which is valid only for inviscid flows. As shown by XXD97, however, the flow-force balance is insensitive to the choice of the control volume—the total flow-force is essentially constant for all values of x in all numerical solutions.

4. COMPARISON OF NUMERICALLY SIMULATED DENSITY-CURRENTS WITH THEORY

All numerical simulations reported in the present paper are carried out to a non-dimensional time $T = 36$. Ensemble time-averages are produced, for simulated fields over the period $T = 12$ to $T = 18$ at a sampling interval of 0.5. To avoid spatial smoothing caused by current propagation, the instantaneous fields are translated in x before averaging, so that their frontal noses collocate with the nose at time $T = 12$. The instantaneous fields at $T = 12$ and the time-averaged fields from selected experiments will be shown. In general, the simulated flow in the head region is already rather steady by $T = 12$.

(a) *Cases with positive low-level shear and varying upper-level shear*

The results from the first five experiments listed in Table 1 are discussed in this section. The shear of the upper-layer varies from +2 to −2 by intervals of one. The theoretical model predicts that the depth of the steady-state density-current (h) increases monotonically with the increase in the upper-level shear (Fig. 4(a)). The density-current depth is 0.32 for $\beta = -2$, for example, but 0.79 for $\beta = +2$ (see Table 1).

Figure 7 shows the wind vector and buoyancy fields at $T = 12$ from the five experiments. Since the initial flows and density currents are configured to reflect the theoretical far-field solutions, the simulated density-currents are expected to remain quasi-stationary relative to the model grid so that the front locations remain close to $x = 0.0$. This is indeed true in all five cases. Between $T = 0$ and $T = 12$, in five cases, the front retreats for distances between 0.010 and 0.019. The distance is generally larger for shallower currents, and, therefore, the retreat faster. The retreat of the front reduces the flow-relative propagation-speed, and the relative errors are between 1% and 4.7% for the five experiments, with the error being largest for experiment L1UM2. The absolute error is also largest for L1UM2 (Table 1). This seems to be due to the *relatively* large frictional effect imposed on the density current by the upper-level rearward flow.

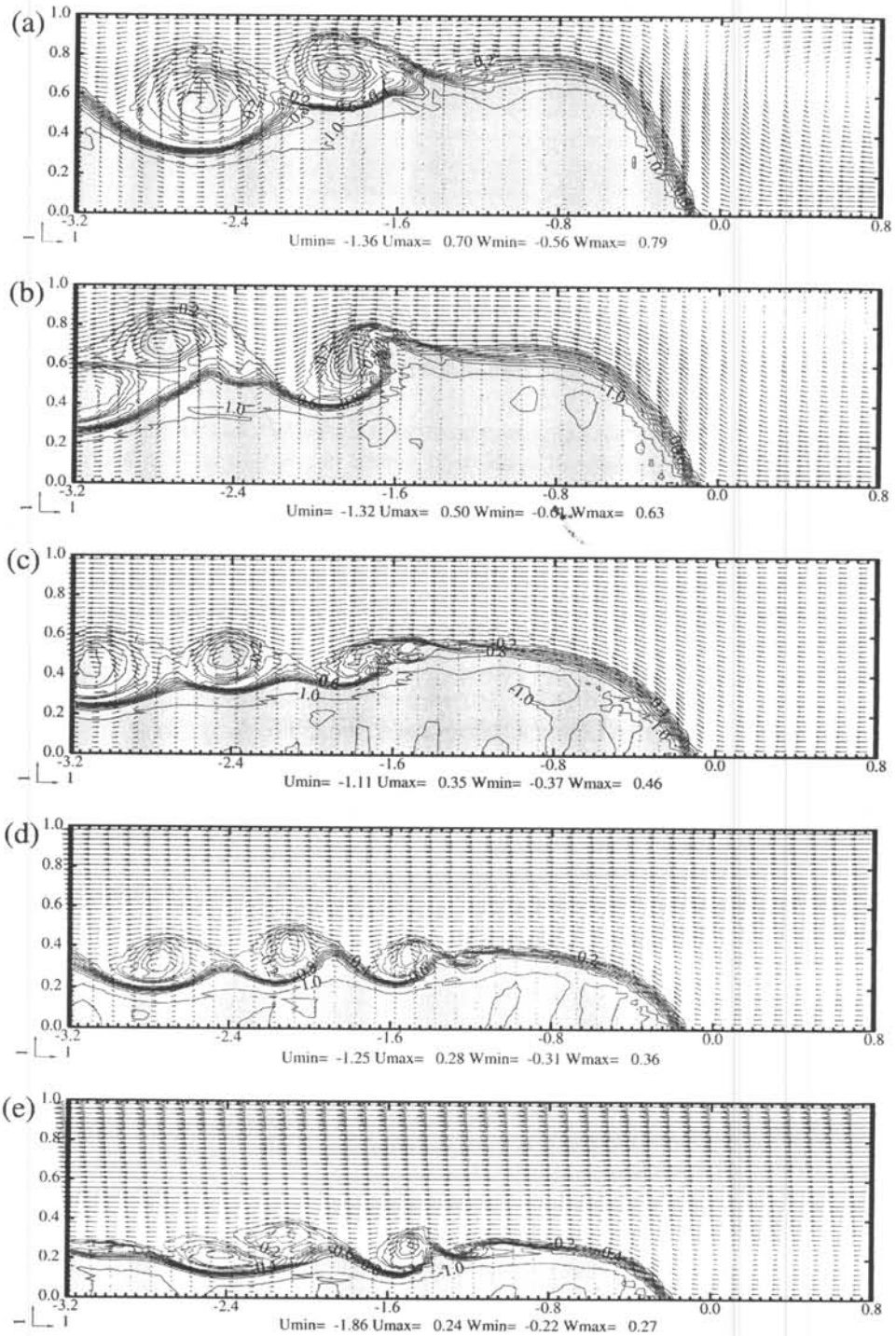

Figure 7. Instantaneous nondimensional velocity and buoyancy (density) fields at $T = 12$ (20 minutes model time) in a nondimensional co-ordinate for the first five experiments (see Table 1), with constant positive low-level shear ($\alpha = 1$) and five different values of upper-layer shear β: (a) L1U2, $\beta = 2$; (b) L1U1, $\beta = 1$; (c) L1U0, $\beta = 0$; (d) L1UM1, $\beta = -1$; (e) L1UM2, $\beta = -2$. The contour interval for buoyancy is 0.1. Other plotting conventions are as in Fig. 6.

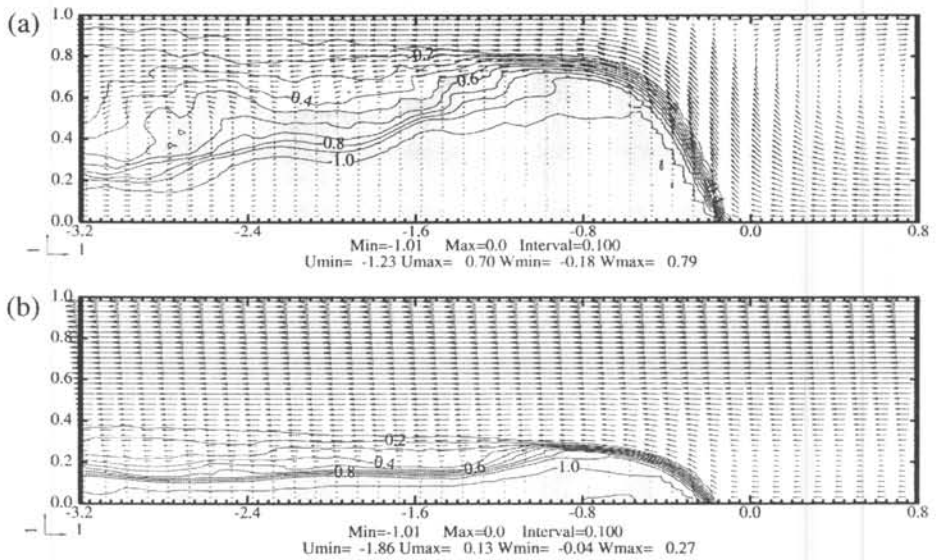

Figure 8. Ensembles of wind and buoyancy fields averaged over the interval $T = 12$ to $T = 18$, for experiments one and five (see Table 1), with constant positive low-level shear ($\alpha = 1$) and two different values of upper-layer shear β: (a) L1U2, $\beta = 2$; (b) L1UM2, $\beta = -2$. For the ensemble average, the fields are sampled at intervals of $T = 0.5$, and the frontal nose is at all times shifted to the nose location at $T = 12$ before averaging. As in Fig. 6, the plots are in nondimensional space. Panels (a) and (b) are the time-averaged counterparts of Fig. 7(a) and Fig. 7(e) respectively.

Measured from the -0.5 buoyancy contours, the height of the simulated density-current head for each of the experiments is given in Table 1. To compare the modelling results with those of the theoretical model, the control volume is chosen between a location upstream where the flow is little influenced by the density current and another in the head region where the flow is more or less horizontal and the turbulent activity is weak. The general dependency of the height on the upper-level shear is well reproduced, and the relative errors are in the range of 4% to 11%. In all cases, the numerical model gives a lower value for the height of the current than the theoretical value. This under-prediction was also observed in the numerical experiments of XXD96 and XXD97, and is believed to be caused by eddy viscosity in the simulated flows and consequent energy loss.

Strong shear at the density-current interface causes pronounced KH billows in the instantaneous fields. These eddies originate from the head region, where strong baroclinicity resulting from the strong horizontal density-gradient generates positive vorticity. However, these eddies remain small when they are advected rearward along the interface in the head region, but grow large to the rear of the head and result in significant density mixing. The behaviour of these eddies has been discussed in more detail by XXD97.

The steady-state flow is better depicted by the time-averaged fields for experiments L1U2 and LlUM2 (Fig. 8). The time-averaged shape of the current head and the sharpness the frontal interface in the region are very close to those at instantaneous times (Fig. 7). This again suggests that the flow in the head region is very steady. The interface behind the head region appears diffused due to the effects of transient eddies.

In Fig. 8(a), an overturning branch exists at the upper-levels ahead of the density current, while in Fig. 8(b), there is only one front-to-rear jump branch. The overturning

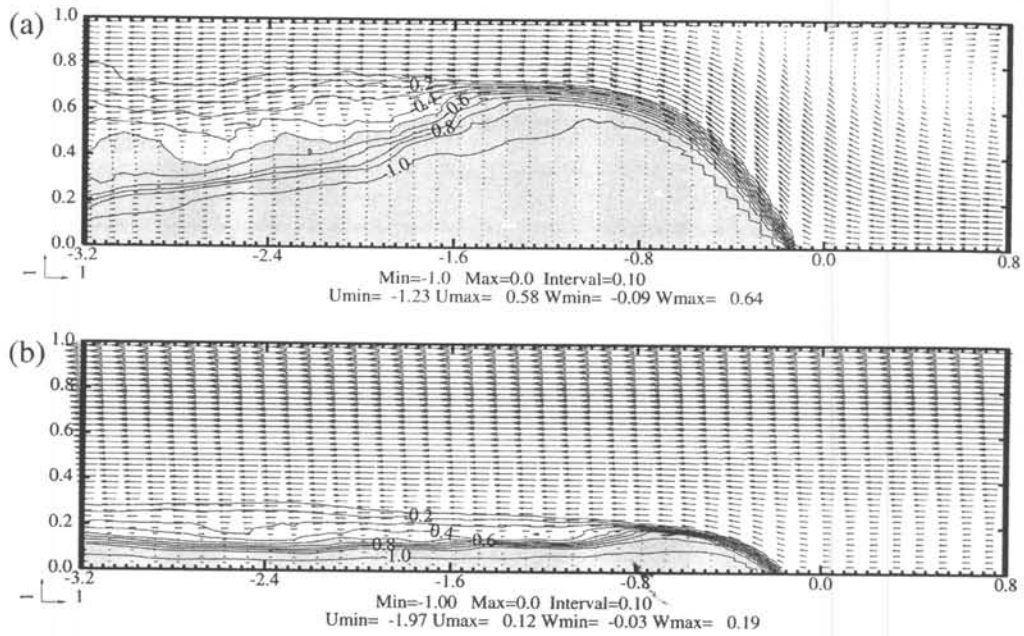

Figure 9. Time-averaged fields as Fig. 8, but for experiments six and seven (see Table 1), with zero low-level shear ($\alpha = 0$) and two different values of upper-level shear β: (a) L0U2, $\beta = 2$; (b) L0UM2, $\beta = -2$.

is also seen in the instantaneous fields for experiments L1U2 and L1U1 (Fig. 7(a,b)). As discussed in section 1, flow overturning is not permitted when the upper-level flow is constant. It is an added and often-observed feature with the introduction of upper-level shear, and it agrees with results from our idealized model discussed in subsection 2(c).

Figures 7 and 8 have axes which are scaled to represent the correct physical proportions of the density current in nondimensional space. They show that the slopes of the simulated fronts at the nose are close to 60°, in agreement with theory (X92, XM94). Away from the surface, the slope of the front generally becomes steeper with increasing upper-level shear. In this respect, upper-level shear and low-level shear play similar roles.

(*b*) *Cases with zero low-level shear*

In experiments L0U2 and L0UM2 (Table 1), the low-level shear is zero while the upper-level shears are 2 and -2, respectively. These two experiments differ from L1U2 and L1MU2 only in the value of low-level shear. According to the theoretical model (Fig. 4), for the same upper-level shear, the steady-state current is deeper for positive than for zero low-level shear (0.79 versus 0.72 for $\beta = 2$, and 0.32 versus 0.25 for $\beta = -2$ when $d_0 = 0.2$, see Table 1). These results are supported by our numerical experiments (compare Fig. 9 with Fig. 8). Table 1 gives the simulated current-heights and propagation speeds for these two experiments, again agreeing well with the theoretical model.

Note, too, the considerable difference in density-current depth between L0U2 and L0UM2 (Fig. 9), even though, in both cases, the shear is zero in the lower $0.2H$ depth where the flow interacts directly with the leading edge of the current. In L0U2, where the upper-level shear is positive, the current head is deep and the frontal interface steep with overturning ahead of it, whereas in L0MU2, where the upper-level shear is negative, the

current head is shallow and the vertical circulation at the front much weaker. This result is important for our understanding of the role of low-level versus deeper-layer shear in supporting long-lasting convective systems such as squall lines (TMM78; RKW88). The presence of positive shear in the flow at the lowest levels may not be essential (although undoubtedly helpful) in supporting deep updraughts. The speed difference between the sub-cloud and cloud-layer flows may be more important (TMM78; Xue 1990). Such inferences are relevant because, in mature squall-line systems (e.g. Houze *et al.* 1989), the interaction between the warm upward branch of circulation (updraught) and the potentially cold (in terms of equivalent potential temperature) downward branch (rear-to-front flow and downdraught) should be governed by dynamics similar to those in our density-current model.

(*c*) *The effect of low-level shear*

We saw in section 1 and subsection 4(b) that the interaction between the density current (thunderstorm outflow) and the environmental shear is important for long-lasting convective systems such as the squall line. It is so because, to a large extent, the cold-pool strength and inflow shear control the strength and orientation of the updraught forced at the frontal zone. For these reasons, consider further the vertical-velocity fields from experiments with different upper- and low-level shear.

We have seen that the density current is deeper for larger positive low-level shear; at the same time, the frontal slope is also steeper. Figure 10 shows that for the same positive upper-level shear ($\beta = 2$), the updraught is about 24% stronger when $\alpha = 1$ than when $\alpha = 0$. Similar behaviour is also observed with negative upper-level shear ($\beta = -2$ in Fig. 11). The difference is about 42% between $\alpha = 1$ and $\alpha = 0$, when $\beta = -2$. In the latter case, the density currents are much shallower and, so, more strongly affected by the magnitude of the low-level shear. In short, a more vigorous and erect updraught is favoured when the low-level shear is positive and large, irrespective of the sign of the upper-level shear. Positive shear therefore provides strong forcing that may trigger or sustain convection.

5. Conclusion and discussions

In the present paper, the two-fluid model of idealized density-current in low-level shear (Xue *et al.* 1997) has been further extended to include variable upper-level shear. This extension gives more flexibility in the specification of inflow profiles. Far-field solutions are determined from the conservation of mass, momentum (flow force), vorticity and the conservation of Bernoulli energy (function) along streamlines for steady-state inviscid flows. It is found that the upper-level shear plays a role similar to the low-level shear in controlling the depth of steady-state density-currents. In most cases, larger positive upper-level shear supports deeper density-current and steeper frontal slope. It is also found that when the low-level shear is weak and upper-level shear occupies about half the domain depth, larger positive shear can result in shallower density-currents (Fig. 4(b)). This behaviour was not found in earlier models for flows with either constant shear or with shear only at low levels. Furthermore, when the upper-level shear varies, overturning flow develops ahead of the density current. This was not possible in the model of XXD97, in which the upper-level flow was assumed to be constant.

Time-dependent numerical experiments are conducted for a range of upper- and low-level shears. The depth and propagation speed of the simulated density-currents are found to agree very well (typically to within a few per cent) with predictions by the

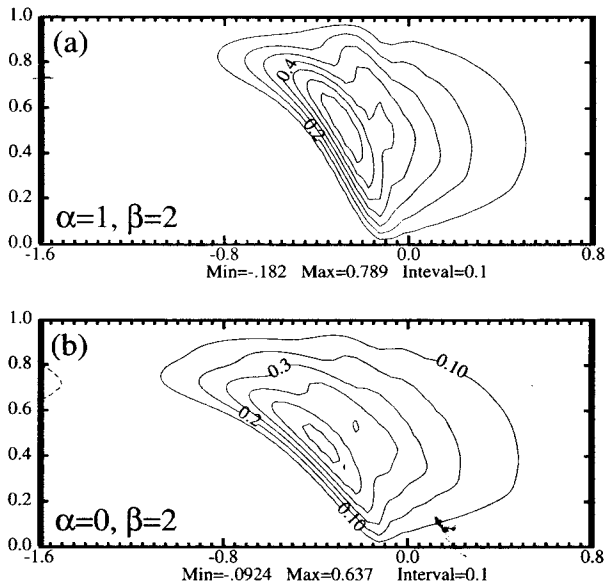

Figure 10. Time-averaged field of vertical velocity w from experiments one and six (see Table 1), in which moderately strong positive shear is constant at upper levels ($\beta = 2$) and the low-level shear takes two different values: (a) L1U2, $\alpha = 1$; (b) L0U2, $\alpha = 0$. Panels (a) and (b) correspond to the time-averaged flow fields in Fig. 8(a) and Fig. 9(a) respectively.

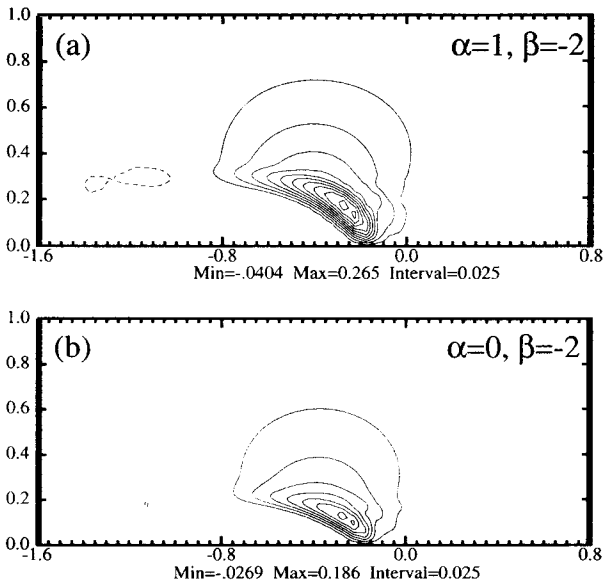

Figure 11. Time-averaged field of vertical velocity w, as Fig. 10, but from experiments five and seven (see Table 1), in which the upper-level shear is negative and constant ($\beta = -2$) and the low-level shear takes two different values: (a) L1UM2, $\alpha = 1$; (b) L0UM2, $\alpha = 0$. Panels (a) and (b) correspond to the time-averaged flow fields in Fig. 8(b) and Fig. 9(b) respectively.

idealized theoretical model in spite of the presence of transient eddies behind the current head in the numerical simulations.

Both theoretical and numerical results show that when the shear in the lowest layer is identically zero, the density-current depth is much greater when the upper-level shear is positive and large. This result may have important implications for understanding the role of low-level versus deeper layer shear in supporting long-lasting squall-lines. The presence of positive shear in the flow at the lowest levels may not be essential in supporting deep updraughts. The difference in the flow speeds between the sub-cloud and cloud layers may be more important.

As pointed out in section 1, the density currents studied here are subject to the limitation that the flow is restricted by a rigid upper boundary. Typically, the presence of this rigid lid forces the flow above the density current to run through a narrow channel, therefore reducing the pressure (based on Bernoulli energy-conservation) in the region. As a result, a deep density current is supported. It is envisaged that, in the real atmosphere, a strong inversion layer or the tropopause act to some extent like a rigid lid in channelling the flow underneath. Indeed, a set of experiments has been completed in which a stable layer with varying degrees of stability replaces the rigid lid. For a stability typical of an isothermal layer, the flow solution below is only quantitatively different from those under a rigid lid. The detailed results will be reported elsewhere.

If we do regard the rigid lid as the tropopause, the atmospheric density-current in the form of thunderstorm outflow can almost never reach more than a third of the tropospheric depth, because of the limitations of the vertical thermodynamic structure and hence of the cold-air supply. The real atmospheric density-current has to be highly turbulent. To address this issue partly, XXD97 conducted an experiment (SLSA), where the environmental shear was strong enough to support a deep current with a steep frontal slope while the cold air supply was insufficient for it to reach the steady-state depth. Even though the flow was highly turbulent and the cold pool was shallow, the numerical solution still showed a branch of deep jump-flow, with the envelope of cold air and frontal slope more or less agreeing with the steady-state solution (see XXD97, Fig. 12). Although, such a single numerical experiment cannot substitute for theoretical solutions with vigorous treatment of energy loss, it provides guidance for problems in less than idealized settings.

In addition, if one extends the definition of density currents to include any flows that include fluids of different densities, one can regard the colder (in terms of equivalent potential temperature in this case) rear-to-front branch of inflow in a well-established squall-line system to be a density current. The density in the colder current does not have to be uniform. The density difference and the dynamic-force balance, together with Bernoulli energy-conservation along the streamlines, determine the overall solution. In this sense, the results from our simple density-current model can be extended to explain squall-line dynamics.

ACKNOWLEDGEMENTS

The author benefited from valuable discussions with Dr Qin Xu. He also acknowledges input from Dr Kelvin Droegemeier. The numerical simulations were performed on the Cray-J90 of the Environmental Computing Applications System (ECAS), University of Oklahoma. This research was funded by NSF Grant ATM91-20009 to the Center for Analysis and Prediction of Storms (CAPS).

REFERENCES

Atkins, N. T., Weekwerth, T. M. and Wakimoto, R. M. 1995 Observations of the sea-breeze front during CaPE. Part II: Dual Doppler and aircraft analysis. *Mon. Weather Rev.*, **123,** 944–969

Benjamin, B. T. 1968 Gravity current and related phenomena. *J. Fluid Mech.*, **31,** 209–248

Carbone, R. E. 1982 A severe frontal rainband. Part 1: Stormwide hydrodynamic structure. *J. Atmos. Sci.*, **39,** 258–279

Chen, C. 1995 Numerical simulations of gravity currents in uniform shear flows. *Mon. Weather Rev.*, **123,** 3240–3253

Droegemeier, K. K and Wilhelmson, R. 1987 Numerical simulation of thunderstorm outflow dynamics. Part 1: Outflow sensitivity experiments and turbulence dynamics. *J. Atmos. Sci.*, **44,** 1180–1210

Fovell, R. G. and Ogura, Y. 1988 Numerical simulation of a mid-latitude squall line in two dimensions. *J. Atmos. Sci.*, **45,** 3846–3879

Houze Jr, R. A., Rutledge, S. A., Biggerstaff, M. I. and Smull, B. F. 1989 Interpretation of Doppler weather radar displays of midlatitude mesoscale convective systems. *Bull. Amer. Meteorol. Soc.*, **70,** 607–619

Liu, C. and Moncrieff, M. W. 1996a An analytical study of density currents in sheared, stratified flow and the effects of latent heating. *J. Atmos. Sci.*, **53,** 3303–3312

1996b A numerical study of the effects of ambient flow and shear on density currents. *Mon. Weather Rev.*, **124,** 2282–2303

Moncrieff, M.W. 1978 The dynamic structure of two-dimensional steady convection in constant vertical shear. *Q. J. R. Meteorol. Soc.*, **104,** 543–567

1992 Organized convective systems: Archetypal dynamical models, mass and momentum flux theory, and parametrization. *Q. J. R. Meteorol. Soc.*, **118,** 819–850

Mueller, C. and Carbone, R. 1987 Dynamics of a thunderstorm outflow. *J. Atmos. Sci.*, **44,** 1879–1898

Rotunno, R., Klemp, J. B. and Weisman, M. L. 1988 A theory for strong long-lived squall lines. *J. Atmos. Sci.*, **45,** 463–485

Simpson, L. E. 1969 A comparison between laboratory and atmospheric density currents. *Q. J. R. Meteorol. Soc.*, **95,** 758–765

Simpson, L. E., Mansfield, D. A. and Milford, J. R. 1977 Inland penetration of sea-breeze fronts. *Q. J. R. Meteorol. Soc.*, **103,** 47–76

Thorpe A.L., Miller, M. J. and Moncrieff M. W. 1982 Two-dimensional convection in non-constant shear: a model of mid-latitude squall lines. *Q. J. R. Meteor. Soc.*, **108,** 739–762

Von Kármán, T. 1940 The engineer grapples with non-linear problems. *Bull. Amer. Math. Soc.*, **46,** 615–683

Wakimoto, R.M. 1982 The life cycle of thunderstorm gust fronts as viewed with Doppler radar and rawinsonde data. *Mon. Weather Rev.*, **110,** 1060–1082

Weckworth, T. M. and Wakimoto, R. 1992 The initiation and organization of convective cells atop a cold-air outflow boundary. *Mon. Weather Rev.*, **120,** 2169–2187

Xu, Q. 1992 Density currents in shear flows—A two-fluid model. *J. Atmos. Sci.*, **49,** 511–524

Xu, Q. and Chang, L.-P. 1987 On the two-dimensional steady upshear-sloping convection. *Q. J. R. Meteorol. Soc.*, **113,** 1066–1088

Xu, Q. and Moncrieff, M. W. 1994 Density current circulations in shear flows. *J. Atmos. Sci.*, **51,** 434–446

Xu, Q., Xue, M. and Droegemeier, K. K. 1996 Numerical simulation of density currents in sheared environments within a vertically confined channel. *J. Atmos. Sci.*, **53,** 770–786

Xue, M. 1990 'Towards the environmental condition for long-lived squall lines: Vorticity versus momentum'. Pp. 1146–1149 in *Preprint of the AMS 16th Conference on Severe Local Storms.* Amer. Meteorol. Soc., Alberta, Canada.

Xue, M., Droegemeier, K. K., Wong, V., Shapiro, A. and Brewster, K. 1995 *Advanced Regional Prediction System (ARPS) Version 4.0 User's Guide.* Available from CAPS, University of Oklahoma, 100 E. Boyd, Norman, OK 73019, U.S.A. [http://www.caps.ou.edu/ARPS].

Xue, M., Xu, Q. and Droegemeier, K. K. 1997 A theoretical and numerical study of density currents in non-constant shear flows. *J. Atmos. Sci.*, **54,** 1998–2019

Zalesak, S. T. 1979 Fully multidimensional flux-corrected transport algorithms for fluids. *J. Comput. Phys.*, **31,** 335–362